Resonance photoemission of $LaCoO_3$(111) and $La_{0.9}Sr_{0.1}CoO_3$(111)

2000 J. Phys.: Condens. Matter 12 9259

(http://iopscience.iop.org/0953-8984/12/44/308)

J. Phys.: Condens. Matter **12** (2000) 9259–9279. Printed in the UK PII: S0953-8984(00)14499-6

Resonance photoemission of $LaCoO_3(111)$ and $La_{0.9}Sr_{0.1}CoO_3(111)$

A G Thomas†‖, W R Flavell†, P M Dunwoody†, C E J Mitchell†¶, S Warren†, S C Grice†, P G D Marr†, D E Jewitt†, N Khan†, V R Dhanak‡, D Teehan‡, E A Seddon‡, Kichizo Asai§, Yoshihiko Koboyashi§ and Nobuyoshi Yamada§

† Department of Physics, UMIST, PO Box 88, Manchester M60 1QD, UK
‡ CLRC, Daresbury Laboratory, Warrington, Cheshire WA4 5AD, UK
§ The University of Electro-Communications, 1-5-1, Chofugaoka, Chofu, Tokyo 182-8585, Japan

E-mail: tom@fs2.phy.umist.ac.uk

Received 30 May 2000, in final form 4 September 2000

Abstract. Resonant photoemission performed at the SRS Daresbury Laboratory is used to investigate the temperature- and doping-dependent spin states in single crystal $LaCoO_3(111)$ and $La_{0.9}Sr_{0.1}CoO_3(111)$. In an initial study, the surface reactivity of the $LaCoO_3(111)$ surface is investigated using H_2O as a probe molecule. The results are used to interpret changes which may occur in the spectra as a function of time and temperature in UHV, due to surface reactions. This allows us to distinguish effects on the valence band spectra due to spin changes as a function of temperature. The temperature dependence of low binding energy features primarily associated with Co in the low spin (LS) state in $LaCoO_3$ is investigated in detail. In particular, the intensity and onset energy of the Co 3p $\rightarrow$ 3d resonance associated with these features is measured at small binding energy intervals. Delayed resonance onset associated with the LS state is consistently observed. This is used to locate the separate contributions of the low spin and higher spin states to the low binding energy spectrum. We find the contribution due to the LS state lies around 1 eV to lower binding energy than that due to higher spin states in $LaCoO_3$. In contrast, we find the spectrum of $La_{0.9}Sr_{0.1}CoO_3(111)$ to be invariant with temperature, with no delayed resonance effect. The data are discussed in the light of recent models for the spin transitions, including the two stage spin-state model involving an intermediate spin state. Simulation of the temperature variation of the valence band spectra of $LaCoO_3$ using this model provides good agreement with experiment.

1. Introduction

$LaCoO_3$ is of great technological interest e.g. as a solid fuel cell and a catalytic material [1, 2]. These properties may be further enhanced by the substitution of the La ion by Sr and Co by Cu [2]. In addition to the technological interest there is also much investigation of the unusual magnetic and electronic properties of the doped and undoped $La_{1-x}Sr_xCoO_3$ series of compounds, in particular the large magneto-resistive anomalies exhibited by the Sr doped compounds (e.g. [3–15]).

In the undoped compound (i.e. $LaCoO_3$) there is a temperature induced transition at ~90 K from a non-magnetic semiconductor to a magnetic state [3, 16, 17]. The crystal field splitting,

‖ Author to whom correspondence should be addressed.
¶ Present address: New Chemistry Laboratory, University of Oxford, South Parks Road, Oxford OX1 3QT, UK.

0953-8984/00/449259+21$30.00

10 Dq, is just large enough to overcome the intraatomic exchange interaction, J, which favours aligned spins and therefore a high spin (HS) state ($t_{2g}^4 e_g^2$: $5T_2$), so that $LaCoO_3$ is in the low spin (LS) state ($t_{2g}^6 e_g^0$: $1A_1$) below this temperature. It was originally thought that this transition involved a gradual low to high spin transition as a function of temperature. However, the occurrence of an electronic transition at ∼500 K has led to much debate about and study of the exact nature of the spin state in $LaCoO_3$ [18–25]. Abbate *et al* concluded from x-ray absorption and x-ray photoelectron spectroscopies on single crystal samples that $LaCoO_3$ is in a highly covalent LS state up to 300 K on the grounds that neither the XAS and XPS spectra undergo a change in a temperature range of 80 to 300 K [19]. Below 100 K, direct magnetic measurements have confirmed the compound exists in a low spin state [3, 16, 17]. However, a study of $SrCoO_3$ [26] and recent calculations on the occupation of states in $LaCoO_3$ suggest the transition at 100 K is to an intermediate spin (IS) state, $3T_1$, with a mixture of $t_{2g}^5 e_g^1$ and $t_{2g}^5 e_g^2 \underline{L}$ states (where $\underline{L}$ indicates a ligand hole state). In a purely ionic model, this state would never be the lowest energy state; this would be either LS or HS depending on the balance between 10 Dq and J. However, the IS state is thought to be lowered in energy relative to HS by very strong Co 3d–O 2p hybridization [18, 25]. This reflects the general tendency in oxides with unusually high valence state transition metals to undergo a ground state ligand to metal electron transfer mechanism thus reducing the valence of the metal [24, 26]. In the case of $LaCoO_3$ this corresponds to d^6 to $d^7\underline{L}$ [25]. The lowering in energy of the IS state through hybridization gives a possible explanation for the LS–IS transition.

The intermediate spin state would be expected to be metallic. In fact, $LaCoO_3$ is insulating below ∼500 K. It has been suggested that this is due to magnetic orbital ordering, which leads to the states being pulled back from the Fermi level [25]. At 500 K there is a second transition to a metallic state, which Korotin and co-workers suggest is due to the loss of orbital ordering allowing the broad e_g bands to cross the Fermi level [25]. These authors suggest the high spin state is at such a high energy above the intermediate state it cannot be reached until temperatures well in excess of 500 K. More recently it has been shown via neutron scattering experiments that the 500 K transition entails an anomalous lattice expansion, which implies a second spin-state transition from an IS to HS state [17]. The data were interpreted in terms of a three spin-state model (LS, IS, HS), with gradual transitions between LS and IS, and then between IS and IS/HS as the temperature is raised [17]. The results of this study suggest that the energy gap between the IS and HS states decreases as the temperature is raised, eventually leading to the formation of a mixed IS/HS state. However, recent calculations using the self-energy corrected Hartree–Fock approximation (for long range spin and orbital orders at 0 K) have suggested that the IS and HS states have very similar energies, both around 1 eV higher than the LS phase [27].

In contrast to the undoped compound, $La_{1-x}Sr_xCoO_3$ (where $x \geqslant 0.08$) was originally thought to exist in a high spin state at all temperatures due to lattice expansion induced by the dopant Sr ions [23]. However it has been suggested more recently from cluster calculations that this compound exists in an IS state [28]. Interpretation of the magnetic properties is further complicated by much recent evidence for an inhomogeneous distribution of the dopant Sr ions [12, 13], leading to hole-rich ferromagnetic regions within a hole-poor semiconducting matrix at low values of x ($x \leqslant 0.25$) [12]. However, it appears that the holes introduced by Sr doping stabilize the IS state to very low temperatures [12, 29], and a large decrease in the unit-cell volume and mean Co–O bondlength associated with the disappearance of e_g electrons is observed only below 2 K for $0 < x \leqslant 0.1$ [12].

In this work we have studied spin-dependent effects in the photoemission of both single crystal $LaCoO_3(111)$ and single crystal $La_{0.9}Sr_{0.1}CoO_3(111)$ over a wide temperature range.

It is important in this work to distinguish effects in the photoemission spectra which are due to changes in Co spin state from those which arise due to the degradation of the surface, which may occur as a function of time or temperature in UHV. For this reason, we begin by studying the surface reactivity of the $LaCoO_3(111)$ surface both *in vacuo* and using H_2O as a probe molecule. This aids us in the interpretation of changes occurring in the valence band spectra as a function of temperature. Resonant photoemission at the Co 3p $\rightarrow$ 3d threshold is studied in detail as a function of temperature and binding energy for both $LaCoO_3(111)$ and $La_{0.9}Sr_{0.1}CoO_3(111)$. This complements previous low temperature studies of $LaCoO_3$ [30]. The data are discussed in the light of recent models for the spin transitions in $LaCoO_3$.

2. Experiment

The single crystals were grown by a lamp image floating zone method. Laué back reflection from the $LaCoO_3$ crystal showed the crystal to be slightly twinned as a result of the rhombohedral distortion of the perovskite lattice ($\alpha = 90.7^\circ$) [23]. Simulations of the expected Laué patterns performed at the CLRC Daresbury laboratory, using the Lauegen program [31] showed the best agreement with the (111) face. Clean surfaces of typically a few mm^2 were prepared by cleaving using a VSW crystal cleaving anvil or scraping with a clean diamond file in UHV at a pressure of better than 3×10^{-10} mbar. In general, the best experimental resolution was obtained from cleaved surfaces, and angle-resolved spectra (not shown) showed small valence band dispersions. We regard the scraped surfaces as effectively angle integrated. As the crystals were very small (3 mm $\times$ 3 mm $\times$ 5 mm typical dimensions), it was generally not possible to anvil cleave any one crystal more than once. The cleaned sample surfaces were homogeneous, and surfaces could be re-established reproducibly on scraping. Sample cleanliness was checked by monitoring the evolution of the contamination peaks at around 9.2 eV [28] and 5.1 eV likely to be due to surface OH adsorption. This is discussed in further detail below. The sample was recleaved or rescraped at regular intervals, although in general, this was avoided within data sets, to avoid the creation of artefacts.

The photoemission measurements were performed at the CLRC Daresbury Laboratory using the grazing incidence monochromator (20 eV $\leqslant h\nu \leqslant$ 280 eV) on beamline 6.1, the toroidal grating monochromator (15 eV $\leqslant h\nu \leqslant$ 90 eV) on beamline 6.2 and the spherical grating monochromator (15 eV $\leqslant h\nu \leqslant$ 220 eV) on beamline 4.1. Photoemitted electrons were analysed using a μMott detector in a spin integrated mode (essentially an HA50 rotatable hemispherical analyser) on beamline 6.1, and an ADES 400 rotatable hemispherical analyser fitted with a 1 mm aperture (angular acceptance $\pm 2^\circ$) on beamline 6.2. On beamline 4.1 measurements were made using a Scienta 200 mm fixed hemispherical analyser. The resolution (monochromator + analyser) for energy distribution curves (edcs) was 0.16 eV for the data recorded on beamline 6.2, approximately 0.25 eV for those from beamline 6.1 and 0.20 eV for station 4.1. Constant initial state (CIS) measurements were made using beamline 4.1. Here the proportion of second order radiation at 60–70 eV photon energy is estimated to be around 8%. The photon energy reproducibility using the SGM is around 10 meV.

The position of the Fermi energy was established by collecting spectra from the cleaned metal sample plate in contact with the samples. Some care was taken to investigate possible sample charging effects. Significant charging effects were observed for $LaCoO_3$ below 130 K (evidenced by distortion and shifting of the spectral features to higher binding energy). Meaningful data could not be recorded below this temperature. In particular, we found that CIS data taken below this temperature were not reproducible, as the degree of charging was affected by the photon flux. However, Sr doping significantly improves the conductivity, and

no charging effects were observed for $La_{0.9}Sr_{0.1}CoO_3$ down to 25 K (the lowest temperature investigated here). Some care was taken to ensure the reproducibility of data taken at different temperatures, given the contamination problems referred to above. All the data were collected several times using different surfaces (and in some cases different beamlines). In particular, it was established that low temperature spectra were reproducible after heating to high temperatures in general, unless the surface was heated to >485 K, when the onset of rapid degradation was seen.

In the adsorbate studies doubly distilled, freeze degassed water was admitted to the vacuum chamber via a high precision leak valve. The exposure in langmuirs (1 L = 10^{-6} Torr s) was estimated from the chamber ion gauge. The sample was cooled to around 130 K before dosing then gradually warmed to room temperature. Spectra were recorded at intervals during the heating process.

3. Results and discussion

3.1. General features of the valence band spectra and adsorbate studies

All spectra are normalized to the photon flux, by means of a tungsten grid placed in the beamline, and aligned on the binding energy scale to a Fermi edge spectrum recorded from the clean sample plate. Figure 1 shows energy distribution curve (EDC) spectra of cleaved $LaCoO_3(111)$. The spectra are in good general agreement with those recorded from polycrystalline samples [18, 19, 32]. The spectra show a number of features which may be related to the cluster calculations of Saitoh *et al* [18] in the region of the main valence band. The Co 3d photoemission spectra calculated by these authors for different spin states (neglecting the O 2p contribution) [18] are shown in the lower part of the figure, and the comparison is discussed in more detail below. The large structure observed at ∼3 eV in the experimental data (feature C) is not present in the calculations as this is derived mainly from the O 2p states [18]. A comparison with the simulated O 2p partial densities of states derived by Saitoh *et al* [18] from the He I spectrum of $LaCoO_3$ indicates that this probably also contributes to the broadening of feature D observed in the experimental data (figures 1 and 4). Other possible contributions to feature D are discussed below. A clearly resolved feature can be observed at a binding energy (BE) of 1 eV in the $LaCoO_3$ spectrum. Although this region has been associated with Co in a low spin, $1A_1$ state [18, 33], cluster calculations suggest there are some contributions from the intermediate spin (IS) and high spin (HS) states in this part of the valence band [18] (figure 1). The sharp cut-off of these states just below the Fermi energy is in agreement with recent LDA + U calculations where orbital ordering is thought to occur resulting in states being pulled back from the Fermi energy in the IS state [25]. The remainder of the valence band (to higher binding energy) is dominated by contributions from the IS and HS spin states and O 2p states [18]. The spectra appear to change significantly with temperature, and the intensity of feature B is attenuated as the temperature is raised. The effect of temperature on the valence band EDC spectra of $LaCoO_3$ and $La_{0.9}Sr_{0.1}CoO_3$ is discussed in section 3.2.

The feature at approximately 9.5 eV (feature E) present in the spectra recorded for both compounds is of some concern particularly given its similarity to the notorious '9.5 eV' peak observed in the spectra of related cuprate superconductors [34]. The peak is observed in some of the spectra recorded from polycrystalline samples of the cobaltates [18, 28, 35] and of single crystal $LaCoO_3$ [19]. Inspection of earlier work suggests that it appears with highest intensity at low photon energies [18], and is generally not observed strongly in valence band spectra recorded using x-ray sources [18, 19, 36, 37]. An anomalous satellite is observed at around

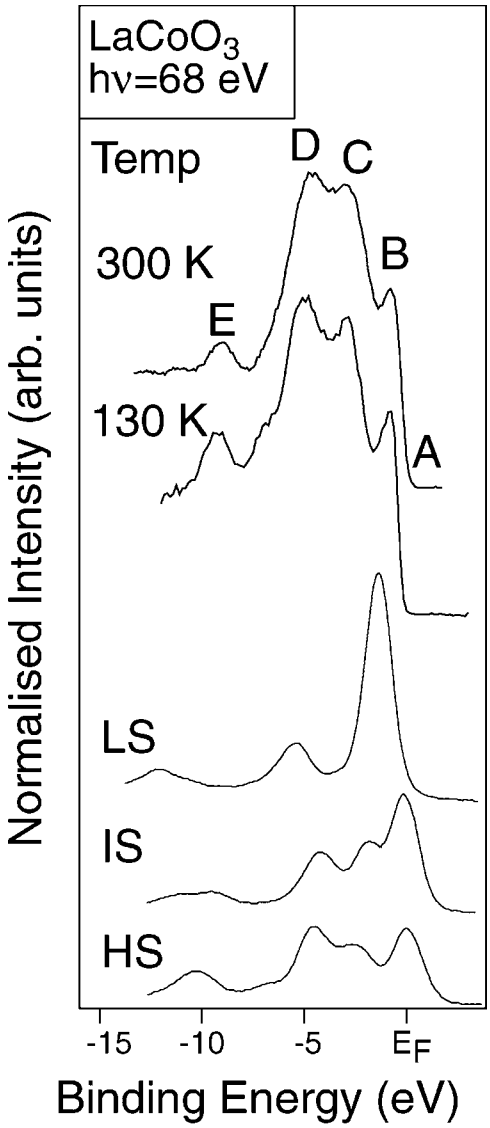

Figure 1. Valence band EDCs recorded from cleaved $LaCoO_3(111)$. The results of cluster calculations [18] for the Co 3d density of states from Co in low spin (LS), intermediate spin (IS) and high spin (HS) states are shown in the lower part of the figure.

this energy in valence band spectra of CoO (Co^{2+}, rather than Co^{3+}, as in $LaCoO_3$) where it has been assigned to a d^6 final state, with the valence band assigned to $d^7\underline{L}$ final states [38]. Cluster calculations suggest that for $LaCoO_3$ the equivalent correlation satellite should also lie at around 10 eV BE [18, 39]. The peak has been shown to undergo a Co 3p $\rightarrow$ 3d resonance in photoemission [35]. We also see a Co resonance associated with the peak in CIS spectra recorded in this work (see section 4, figure 7(b))) confirming some Co 3d character in this part of the spectral function. It seems clear, therefore, that some of the intensity of this feature is intrinsic to the sample. However, the enhancement of the feature at low photon energy [18] and its similarity to the cuprate spectra [34] suggest that some of its intensity may arise as a

result of O-related defects created at the surface following cleaving or through contamination in vacuum. On some occasions, possibly linked to a poor cleave, we have observed changes in the spectral shape as a function of time in UHV. Figure 2 shows such an example. The spectra are recorded at lower photon energy than those in figure 1 to enhance the photoionization cross section of any oxygen states involved in the degradation. Immediately following the cleave, a clear peak is observed at around 9.5 eV binding energy. However after two hours in UHV (1×10^{-10} mbar) contamination or surface changes have occurred, causing a substantial increase in intensity of this feature, and simultaneously that of feature D (at around 5–6 eV BE). This is revealed by the difference spectrum shown in figure 2. The signature of this surface effect therefore appears to be an increase in intensity of both features D and E. This is important to the discussion of the temperature variation of the EDCs in section 3.2. The assignment of the difference spectrum is discussed below.

In order to investigate the degradation process further, we have undertaken a number of studies designed to investigate the reactivity of single crystal and ceramic surfaces of the cobaltates to small molecules likely to be present in the residual vacuum. Figure 3 shows the effect of dosing a single crystal (111) surface of $LaCoO_3$ with H_2O at low temperature. The figure shows the spectrum obtained from a freshly scraped surface at 150 K and the spectrum obtained after dosing with 3 L H_2O. The effect on the spectra of warming the surface after dosing is also shown. Figure 3(b) shows the difference spectra obtained by subtracting the undosed from the dosed spectrum at each temperature, after aligning the spectra at the La 5p core level signals in the range 16–20 eV binding energy. (This is done to correct for any changes in the workfunction of the sample on dosing; we were unfortunately unable to bias the sample during data recording.) In figure 3(b), three peaks at binding energies of 5.8 eV, 8.1 eV and 12.1 eV are evident in the difference spectrum taken at 150 K, together with a feature in the vicinity of B at around 1 eV. At higher binding energy, a broad peak at around 24–25 eV binding energy is also observed, due to O 2s emission from the dosed water.

The appearance of three valence band adsorbate peaks, two of which lie below the valence band of the substrate is typical for nondissociative adsorption of water on metal oxides [40]. By comparison with data for other oxides [34], the three features in the range ∼6–12 eV may be assigned to the $1b_1$, $3a_1$ and $1b_2$ molecular orbitals of undissociated water respectively. The peak separations $\Delta(3a_1–1b_1)$ of 2.3 eV and $\Delta(1b_2–3a_1)$ of 4.0 eV compare well with those of gas phase water (2.1 eV and 3.8 eV respectively [41]). It is now well established that in the case of strong chemisorption to the surface, the $3a_1$ molecular orbital of the adsorbed water experiences a shift to higher binding energy relative to the other orbitals compared with its position in gas phase water [34]. This shift may be up to 1.3 eV [42]. The small shift here suggests that water is weakly chemisorbed to the surface at low temperature. Adsorption appears to cause a loss of spectral resolution. This is particularly apparent for sharp features of the spectrum, such as feature B, which can be seen to be broadened on dosing (see e.g. figure 3(a)). This in turn leads to generation of artefacts when the difference spectra are obtained (figures 2 and 3). Thus the features observed in the difference spectra in the vicinity of B are due to a combination of miscancellation due to broadening on adsorption, on heating, and possible changes in the spin state of the sample. The possible effects of thermal broadening are discussed further in section 3.2.

On warming the surface, further changes are seen in the valence band spectra. In the difference spectrum, the three features due to water adsorption are gradually replaced by two features at binding energies of 4.7 eV and 8.8 eV, and the absolute intensity of the difference spectrum decreases. We associate these features with the 1π and 3σ orbitals of adsorbed OH groups, which appear at 4.9 eV and 9.0 eV binding energy in the spectra of the related layered perovskite $La_{2-x}Sr_xCuO_4$ [43]. Thus, the adsorbed water dissociates as the sample is warmed,

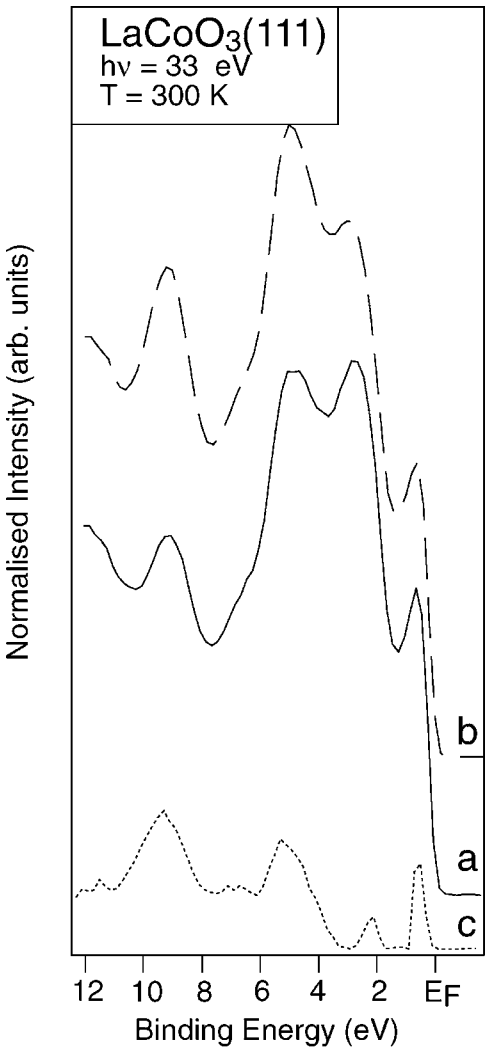

Figure 2. EDCs from $LaCoO_3(111)$ recorded immediately after cleaving (a), and after approximately 2 h in UHV at a vacuum of 1×10^{-10} mbar (b). The difference spectrum (b) − (a) is also shown (c). Spectra are recorded at 33 eV (see text).

leaving surface hydroxide, which is not completely desorbed even at room temperature. The temperature at which dissociation occurs is difficult to estimate from the difference plots, but intensity from the $1b_2$ molecular orbital of water disappears completely between 190 K and 200 K. Careful examination of the initial difference spectrum taken at 150 K shows that the $3a_1$ signal is rather broad, and the $1b_1$ signal has a low binding energy shoulder, suggesting that some OH may co-exist with H_2O on this surface even at low temperature. Recent elegant *ab initio* calculations have demonstrated that this may occur on oxide surfaces [44]. The binding energy positions and energy separation (4.1 eV) of the OH features are in very good agreement with the difference spectrum of the degraded $LaCoO_3$ surface (figure 2), where the two main features are also separated by 4.1 eV. We therefore conclude that the degradation of the surface sometimes observed as a function of time in UHV is due to the formation of surface

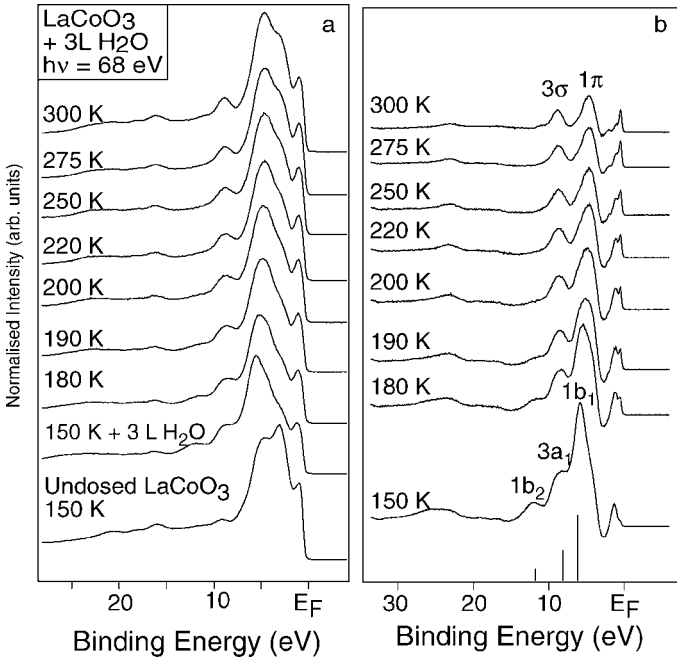

Figure 3. (a) EDC spectra recorded at 68 eV photon energy showing the effect of water adsorption and subsequent warming on $LaCoO_3(111)$. Spectra have been normalized to the beam monitor reading, and aligned on the binding energy scale to the La 5p core level intensity in the binding energy range 16–20 eV. (b) Difference spectra (dosed surface-undosed surface) obtained from the data shown in (a), following water dosing and warming a $LaCoO_3(111)$ surface. The spectra have been normalized to feature C (labelled in figure 1) before subtraction. Assignments to the molecular orbitals of H_2O and OH are given. The molecular orbital positions for gas phase water are shown for comparison along the abscissa. The gas phase BE positions have been shifted so that the binding energy position of the gas phase $1b_1$ peak has been aligned to the $1b_1$ orbital of the adsorbed H_2O.

OH, presumably through adsorption of H_2O from the residual vacuum. The dissociation of water to give OH may be enhanced at the step and defect sites associated with a poor cleave. Preferential dissociation on stepped oxide surfaces has been previously observed for related perovskite oxides such as $SrTiO_3$ [45]. It seems therefore that the freshly cleaved or scraped single crystal is quite reactive to the presence of water. It is interesting to compare our results with metastable atom electron spectra (MAES) of $LaCoO_3$ [35]. As the He atoms used do not penetrate the surface, the technique is essentially sensitive only to the topmost atomic plane of the surface, and will detect any surface deterioration extremely sensitively. We note that both the 'satellite' feature E and a feature around 3.7 eV to lower binding energy appear to be anomalously enhanced using this technique [35], corresponding fairly well with the difference spectrum we observe in figure 2.

It is evident that the surfaces studied are highly reactive in UHV, and may be degraded to varying extents depending on the quality of cleaving or scraping, and the length of time in UHV (as evidenced, for example by a comparison of figure 1 with the undosed spectrum of figure 3). In order to interpret the temperature variation of the valence band EDCs, discussed in the next section, it is necessary to identify the signature of the degradation products in order to distinguish the contamination effects from any effects due to changes in spin state. In this context it is important to note that any increase in surface degradation during an experiment should be accompanied by a uniform increase in intensity of both features D and E.

3.2. Effect of temperature on the valence band spectra

As can be seen from the spectra in figure 1, a number of changes are observed in the spectrum of $LaCoO_3$ as a function of temperature. Most notably, there is a decrease in the intensity of the peak at 1 eV BE as the temperature is increased. This is likely to be caused by depopulation of the LS state at the higher temperature relative to the lower temperature spectrum. Figures 4 and 5 show more detailed investigations as a function of temperature for scraped surfaces of $LaCoO_3(111)$ and $La_{0.9}Sr_{0.1}CoO_3(111)$ respectively. In the case of $LaCoO_3$ (figure 4), it was not possible to record meaningful spectra below 130 K due to charging of the sample. At temperatures above 485 K, the chamber pressure and hence the rate of surface degradation rose to levels where the spectra became dominated by the effects of surface degradation as characterized above. The slight difference in the spectral quality between the spectra presented in figures 1 and 4 is believed to be caused by the different methods of cleaning the surfaces. However, the general features and intensity changes of the two data sets are consistent. It is clear that feature B, which has been associated primarily with Co in a low spin state [18, 33] decreases in intensity with increasing temperature, indicating that the low spin state is becoming depopulated. At the same time we observe an increase in the spectral weight in the rest of the valence band as other spin states become more dominant. The data recorded at 425 K show an increase in intensity of feature D at a binding energy of 5 eV. At 485 K this enhancement of feature D is clearer and is coupled with a decrease in the intensity of feature C. It is clear that these changes are not accompanied by an increase in intensity in feature E (which has a roughly constant intensity throughout). This differs from the pattern for surface decomposition shown in figure 2, where we show that as the surface degrades, both features D and E are enhanced. This, combined with the results of valence band simulations (section 3.3), leads us to attribute the changes in relative intensity of features B, C and D in figure 4 to changes in the spin state of the sample. These changes appear consistent with a three spin-state model involving the IS state, with rather gradual transitions between states, and with more than one state existing at all temperatures. This is generally consistent with neutron diffraction results [17], and is discussed further in the light of resonance experiments described in section 3.4.

In order to confirm that the changes which occur in these spectra are due to spin-state changes, it is necessary to repeat the experiment using an Sr-doped crystal, as this material exists in the same spin state (believed to be IS) at all temperatures accessed by our experiment [12, 28]. For example, it is possible that a significant apparent decrease in intensity in feature B with increasing temperature may be caused simply by phonon broadening of this sharp feature. The possible effect of phonon broadening is difficult to estimate, as, for a polar material, it depends strongly on the difference between the static and high frequency dielectric constants [46], which is not well established in this case. We anticipate that it could contribute several hundred meV to the spectral widths, but as it depends on $(\coth\{h\nu_{LO}/2kT\})^{1/2}$ (where $h\nu_{LO}$ is the longitudinal optical phonon energy) [46], it is not a strong function of temperature. For this system, clear effects on the spectral width appear only to be visible at temperatures in excess of around 500 K [19]. The effect of temperature on the valence band spectra of $La_{0.9}Sr_{0.1}CoO_3(111)$ is shown in figure 5. Compared with the spectra of figure 4, it can be seen that the basic features of the spectra do not change significantly with temperature (although there are small variations which are discussed below). Importantly, we note that the intensity of feature B relative to the maximum at D does not decrease with temperature, and we can thus be confident that the reduction seen for $LaCoO_3$ (figure 4) is due to a depopulation of states at this binding energy, and not merely a consequence of phonon broadening. Secondly, we note that the intensity of feature B for the Sr-doped material is significantly reduced from that of the 130 K $LaCoO_3$, spectrum (figure 4). This is consistent with an LS contribution to

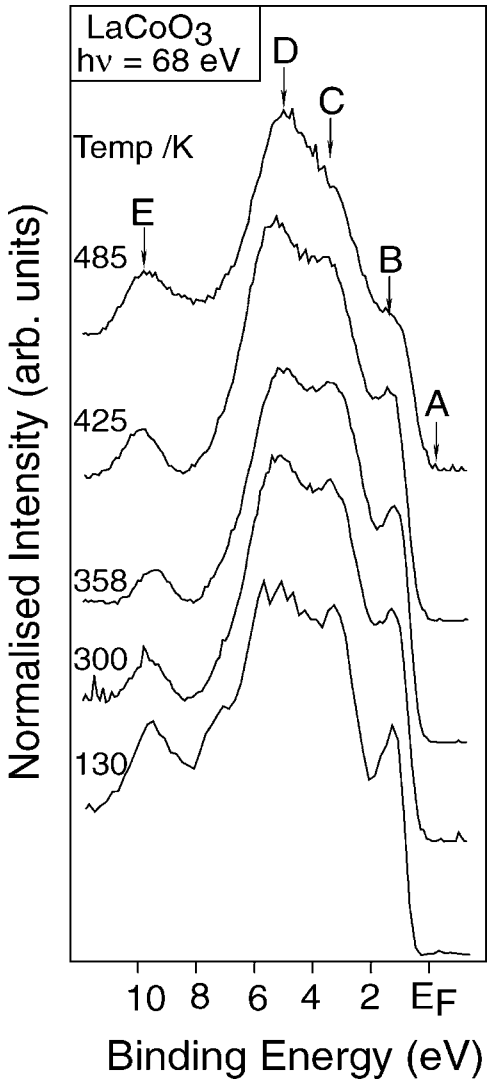

Figure 4. Effect of temperature on the valence band EDC spectrum of scraped $LaCoO_3$(111) recorded at a photon energy of 68 eV, in order of increasing temperature.

this feature in low temperature $LaCoO_3$, which is absent in the Sr-doped material (as the LS state here is stable only below 2 K [12]). Inspection of the cluster calculations (figure 1) [18] shows that all three spin states (LS, HS and IS) should contribute to the intensity of feature B, so we expect the feature to be present in the spectra of the Sr-doped material, but with reduced intensity relative to low temperature $LaCoO_3$, as is observed.

In the light of the discussion in section 3.1, it can be seen that there are some small variations in the extent of surface degradation in this experiment, which cause small variations in the valence band spectra. These are, however, far less significant than the variations due to spin state changes in figure 4. In particular, it is evident in figure 5 that the spectrum recorded at room temperature (300 K) shows a slightly lower intensity at 9.5 eV binding energy than those accumulated at other temperatures. We believe that this is because this was the first spectrum

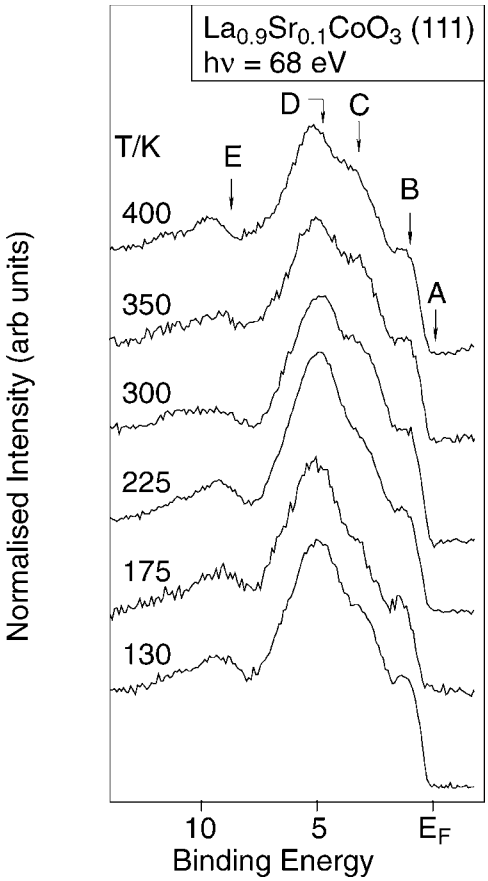

Figure 5. Effect of temperature on the valence band EDC spectrum of scraped $La_{0.9}Sr_{0.1}CoO_3(111)$ recorded at a photon energy of 68 eV. The spectrum at 300 K was recorded first, followed by the remainder in order of increasing temperature.

taken after sample scraping; the remaining data were taken after sample cooling and subsequent warming. At low temperature, the sample has an increased tendency to adsorb water from the residual vacuum, while at the highest temperatures, the surface becomes increasingly unstable to degradation as described above for $LaCoO_3$. This may be compounded by an increase in defects at the surface, in particular loss of surface oxygen.

3.3. Simulation of the valence band spectra of $LaCoO_3$ as a function of temperature

In principle, as cluster calculations for the LS, HS and IS states exist [18], and the relative proportions of these states have been established through magnetic susceptibility measurements [17], it is possible to simulate the valence band spectra expected for $LaCoO_3$ as a function of temperature. These simulations are shown in figure 6. The cluster calculations of Saitoh *et al* have been used to represent the Co 3d density of states for the LS, IS and HS states [18]. The proportions of each state at the temperatures of our experiment are as calculated from the magnetic susceptibility data of Asai *et al* [17], and are shown in table 1. The relative binding energies of the LS, HS and IS contributions are as given by Saitoh *et al*, except that the lowest binding energy feature of the LS spectrum is shifted to lie 1 eV to lower binding

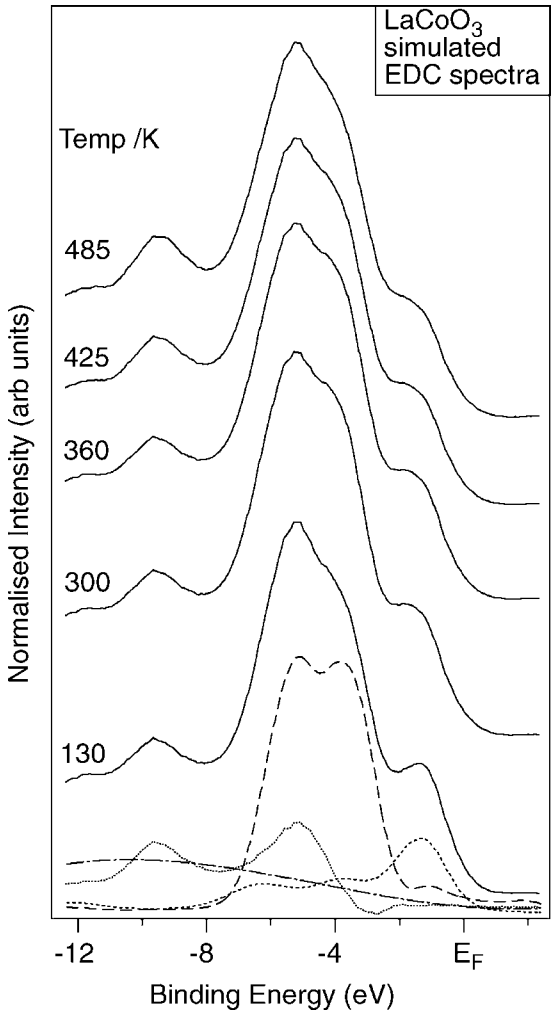

Figure 6. Simulated valence band spectra of $LaCoO_3$ at $h\nu = 68$ eV as a function of temperature. Details of the simulation are given in the text. An example of the contributions to the spectra is shown for the 130 K spectrum. Long dashed line: O 2p density of states from [27], with proportions of the LS, HS and IS states from [17]. Dashed line: Co 3d density of states from [18], with proportions of the LS, HS and IS states from [17]. Dotted line: surface contamination contribution, see text. Dot–dashed line: secondary electron background contribution.

energy than the corresponding features in the IS and HS spectra. The justification for this shift comes from the detailed CIS investigation described in section 3.5, which allows us to determine the relative energy separation of the LS and HS/IS states. Estimation of the O 2p density of states to be included is non-trivial, as has been noted by Saitoh *et al* [18]. The HF + Σ calculations of Takahashi and Igarashi [27] show that this function changes substantially between LS, IS and HS states. We have therefore taken different functions for each state, using the results of the HF + Σ calculations [27], broadened to our experimental resolution, again in the proportions suggested by the magnetic susceptibility measurements (table 1). The Co 3d and O 2p contributions have then been added in the proportions suggested by their relative abundance in the crystal, and their relative photoionization cross-sections at

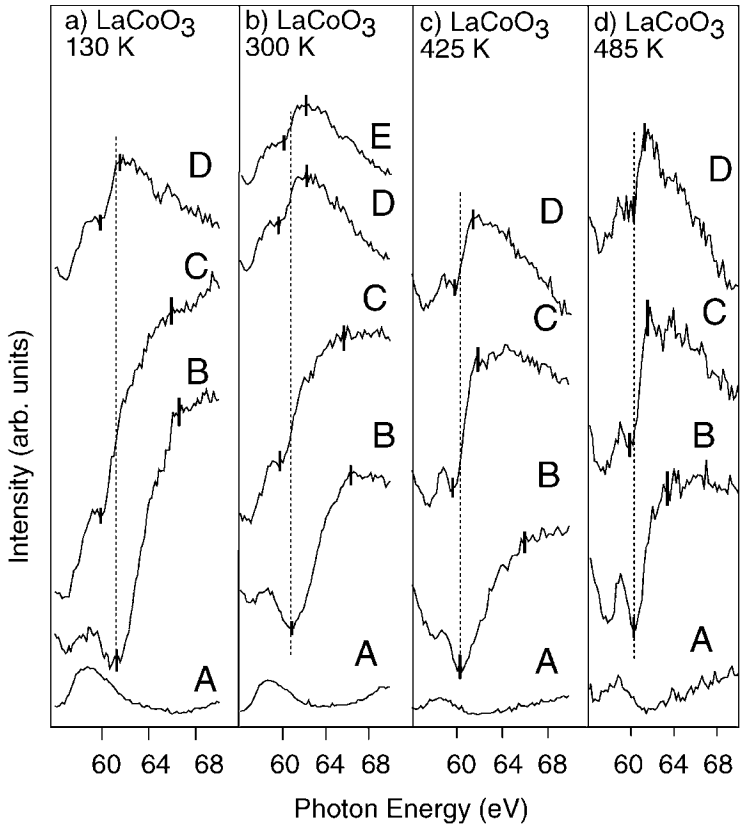

Figure 7. CIS spectra recorded from $LaCoO_3$ (111) at temperatures of (a) 130 K (scraped), (b) 300 K (cleaved), (c) 425 K (scraped) and (d) 485 K (scraped). The spectrum from feature E is included in the 300 K data to show the resonance observed at the 'satellite' position (see text). The dashed lines originating at the resonance minimum of feature B are drawn to emphasize the ∼3 eV shift in resonance position between B and C–E at low temperature. Spectra are normalized to the incident photon flux, and recorded in the order (b), (a), (c), (d).

this photon energy (68 eV) [47]. In order to include the effects of surface degradation, we have used a difference spectrum obtained by subtracting spectra (recorded at 68 eV photon energy) of a freshly scraped surface and the same surface when contaminated. This has been included as a constant contribution at all temperatures, scaled arbitrarily to match experiment at feature E and 130 K. Finally, we have added the third order polynomial background function shown in figure 6 to represent the secondary electron tail, scaled to the background step jump between 0 and 12 eV binding energy in our experimental spectra.

By comparing figures 4 and 6, we can see that there is excellent agreement between simulated and experimental spectra. In particular, the decrease in intensity of feature B with temperature, and its intensity relative to the main valence band are well replicated. The small changes in relative intensity of features C and D are also well replicated. We conclude that the three-state model (with proportions of the states as determined by Asai *et al* [17]) appears to provide a very satisfactory description of the valence band spectra. In particular, the gradual changes in the spectra as a function of temperature are well reproduced, and this is consistent with a model where a mixture of spin states is present at all temperatures accessed in our experiment. As can be seen from table 1, the proportion of the LS state drops rapidly with

Table 1. Occupation of the three spin states at 130, 300, 360, 425 and 485 K, calculated from magnetic susceptibility data [17].

T (K)	LS	IS	HS
130	0.25	0.75	0.00
300	0.10	0.87	0.02
360	0.09	0.86	0.05
425	0.08	0.83	0.09
485	0.07	0.79	0.15

increasing temperature between 130 K and 300 K, but thereafter declines very slowly. The dominant contribution at all temperatures probed is expected to be from the IS state, with the HS contribution becoming significant only above 400 K. As the degradation contribution to the simulations has been taken as constant throughout, it is clear that the changes in the valence band spectra as a function of temperature are due to changes in the spin state of the sample.

3.4. Resonance photoemission studies

In this section, we explore the effect of the spin state of the sample on the Co 3p $\rightarrow$ 3d resonance photoemission profiles. 3p $\rightarrow$ 3d resonant effects are seen for a wide range of transition metal oxides. The processes occurring are described for a general $3d^n$ initial state configuration below. The direct photoemission process may be written:

$$3p^6 3d^n + h\nu \rightarrow 3p^6 3d^{n-1} + e^-.$$

At photon energies larger than the 3p $\rightarrow$ 3d absorption threshold, the direct process is supplemented by initial 3p $\rightarrow$ 3d excitation, followed by super-Coster–Kronig Auger decay:

$$3p^6 3d^n + h\nu \rightarrow \{3p^5 3d^{n+1}\}^* \rightarrow 3p^6 3d^{n-1} + e^-.$$

Resonant effects are attributed to interference between direct and indirect channels. We may therefore expect the observed binding energy of the resonance features to be affected by the initial occupancy of the d orbitals, and the resonance position may therefore reflect the spin state of the sample.

Figure 7 shows constant initial state (CIS) spectra recorded over the Co 3p $\rightarrow$ 3d resonance for $LaCoO_3$, at 130, 300, 425 and 485 K. The binding energy positions chosen for the CIS spectra are labelled in figure 1. All of the CIS spectra show a small resonance at a photon energy of $\sim$59 eV followed by a larger main resonance at energies between 61 and 64 eV with the exception of point A, which shows only the 59 eV feature. This is in agreement with CIS spectra recorded from CoO where the double peaked structure is assigned to transitions from different spin orbital components of the Co 3p initial state [38]. However, the observation of only the small 59 eV feature at point A suggests that it is not an intrinsic part of the resonance structure. EDCs were taken at different photon energies around the resonance energy in order to isolate any contributions from second order radiation, or Auger features. No such features (characterized by apparent dispersion in steps related to the photon energy change when displayed on a binding energy scale) were found. Our discussion therefore centres on the main resonance at $\sim$62 eV. It is clear that the main resonance onsets at position B for the low and room temperature data are at approximately 3 eV higher energy than for the other features. If part of the intensity of the resonance at B derives from low spin Co, then this would be expected as in the low spin state all of the t_{2g} states are full, thus only the e_g states (which according to calculations lie approximately 3 eV above the t_{2g} states [25]) can contribute to the spectrum leading to a delayed resonance onset. In the higher binding energy parts of the

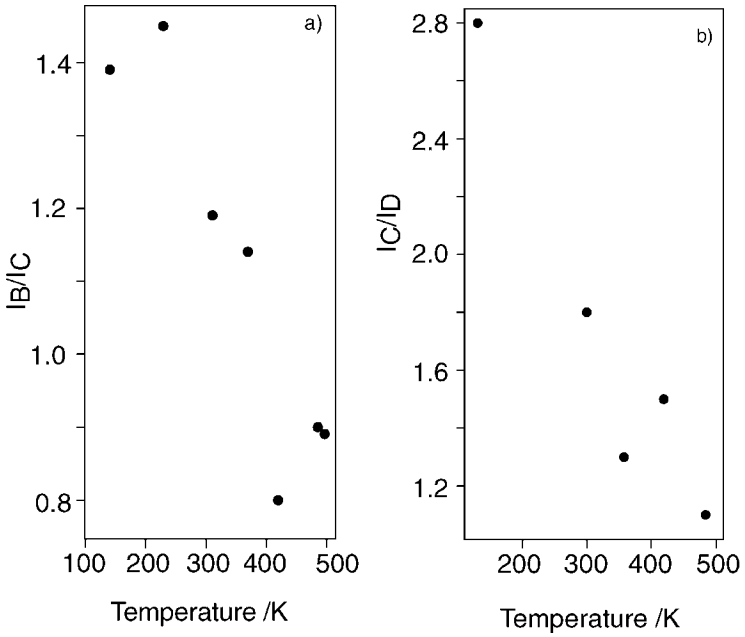

Figure 8. (a) The ratio of intensities of resonance onset, I_B/I_C for features B and C and (b) for features C and D. The resonance edges were normalized to the intensity of feature A to remove any possible discrepancies due to different analysers or sample positions, and the intensities are determined using the markers in figure 7 (see text).

valence band (features C and D) which correspond to Co in intermediate ($t_{2g}^5 e_g^1$ and $t_{2g}^5 e_g^2 \underline{L}$, where $\underline{L}$ represents a ligand hole), and high spin ($t_{2g}^4 e_g^2$) states we now have empty t_{2g} states for the Co 3p electrons to be excited into thus the resonance onset is at a lower energy at these points. The observation of a delayed resonance is therefore a useful diagnostic of the LS state. This concept is used to locate the LS contribution to feature B in section 3.5.

The data recorded at 130 K show the resonance intensity of feature B to be enhanced relative to the other valence band features, presumably as at this temperature the ratio of LS to IS/HS is the highest investigated in this work. This change in the intensity of the resonance edge is shown more clearly in figure 8(a), where the relative intensities of the resonances of features B and C are plotted against temperature. The spectra were normalized to the intensity of the 59 eV resonance of point A in order to remove any differences in the analyser performance/sample positions during data acquisition. The 'before' and 'after' resonance intensities were taken at the points indicated by the markers in figure 7. The gradual decrease in intensity I_B/I_C is suggestive of a gradual transition from the low spin state into other spin states as the temperature increases. Figure 8(b) shows the same information for peaks C and D, where it can be seen that there is also a gradual decrease in the ratio I_C/I_D as the temperature is raised. Given the relative intensities of these features predicted by cluster calculations (discussed above and shown in figure 1), this is consistent with a further gradual transition from the intermediate spin to a high spin state as the temperature is increased.

Figure 9 shows the effect of temperature on the energy of the resonance onset for features B and C (taken as the mid-point of the markers in figure 7). The resonance onset energy of B in $LaCoO_3$ clearly falls as the temperature is increased because as the low spin state is depopulated in favour of other spin states (IS or HS), empty t_{2g} states become available into which the

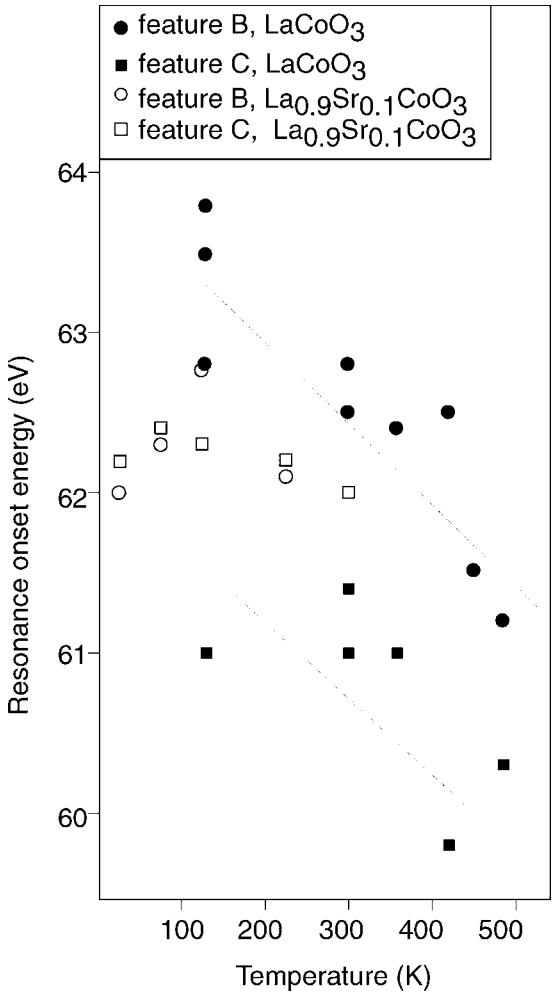

Figure 9. Resonance energy onset for features B and C for $LaCoO_3$ (filled markers) and $La_{0.9}Sr_{0.1}CoO_3$ (open markers) plotted against temperature to show the decrease in resonance onset energy as t_{2g} states become available to the 3p $\rightarrow$ 3d resonance process in $LaCoO_3$. The dashed lines are drawn for heuristic purposes only (see text).

resonance can occur. It is clear that the total drop in energy over the range 130–500 K is approximately 3 eV, which, as stated previously, approximately corresponds to the crystal field stabilization energy. It should be noted that there will also be a contribution from the energy differences in electron correlation and charge transfer effects, depending on the electronic configuration changes occurring between the different spin states (i.e. to account for the fact that in the region of LS the CIS experiment excites an electron into the empty e_g state, whereas in the IS case an electron is excited into a t_{2g} state already containing five electrons and the e_g also contains one or two electrons), thus the measured energy gap we present here may not be purely the crystal field splitting (10 Dq). It should also be remembered that there are some contributions from the IS and HS states under the main feature at B and it is these that allow us to monitor the reduction in excitation energy of B. The dashed lines in figure 9 are therefore for heuristic purposes only as, given the discussion above, we clearly have no reason to expect

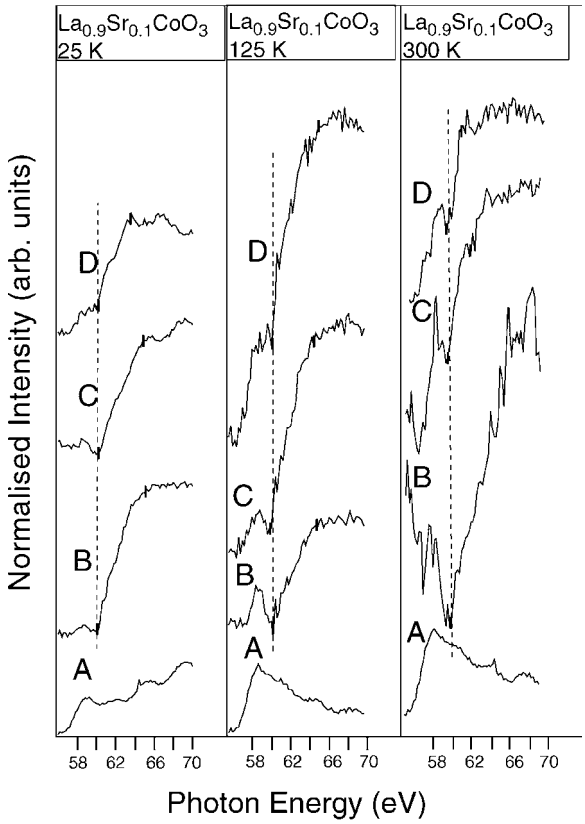

Figure 10. CIS spectra of scraped $La_{0.9}Sr_{0.1}CoO_3(111)$ at 25, 125 and 300 K, recorded in order of increasing temperature. Dashed lines are drawn from the resonance minimum of feature B to guide the eye. There is no resonance onset delay for any of the features even at 25 K.

the changes in resonance onset energy with temperature to be linear. It can be seen from the cluster calculations shown in figure 1 [18] that all three spin states contribute to some extent to the resonance measured at feature B, and this will complicate the temperature dependence; in principle we expect a delayed onset only for the LS state, and not for HS or IS. The calculations predict that the intensity maximum at B for LS is slightly displaced from that for IS and HS. Thus CIS recorded at small binding energy increments across feature B may show different onset behaviour at slightly different binding energy positions, allowing us to separate the LS and IS/HS contributions to the resonance. Experiments designed to probe this possibility are described in section 3.5, below.

Figure 10 shows the CIS spectra recorded from valence band features A, B, C and D (labelled in figure 5 in $La_{0.9}Sr_{0.1}CoO_3$ at temperatures of 25, 125 and 300 K. There is little change as a function of temperature. Most importantly we see no systematic shift in the energy of the resonance onset for feature B (plotted in figure 9), even at 25 K. This, combined with the temperature invariance of the EDC spectra, strongly suggests that the Sr-doped compound is in a constant spin state at all temperatures which in the light of recent data [12, 23, 28] we assign to an IS state. For the reasons discussed above, it is difficult to make direct comparison of the onset energies for the Sr-doped and undoped compounds (as we do not expect the decrease in onset energy of feature B for $LaCoO_3$ to be linear, and there is substantial scatter in figure 9). However, it appears that the resonance onset energies of the Sr-doped compound

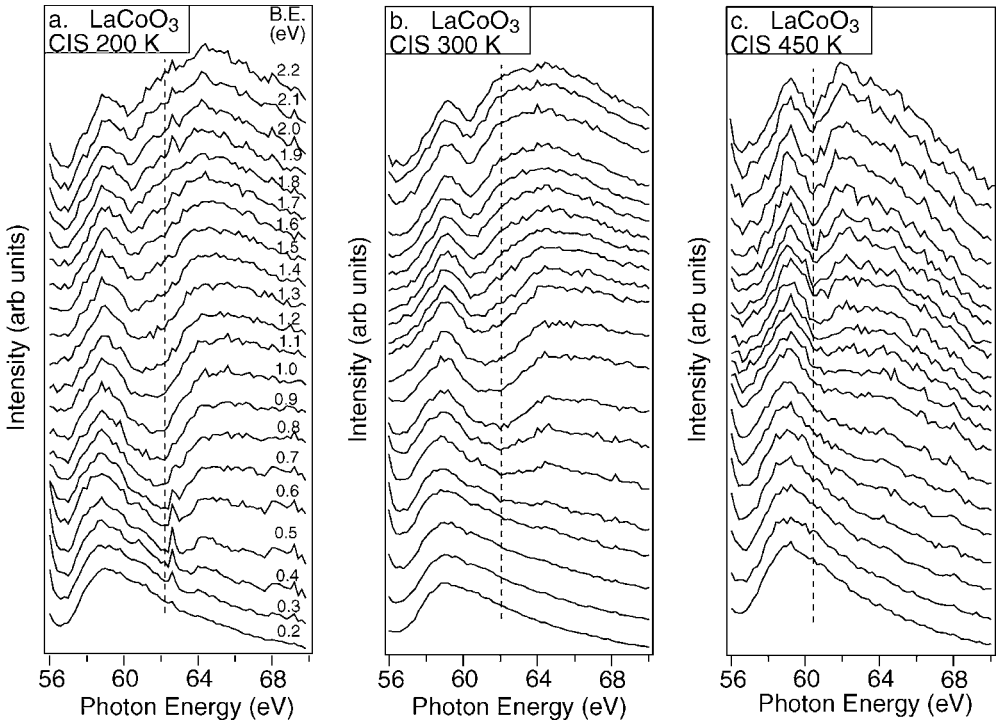

Figure 11. CIS spectra recorded for small binding energy increments across feature B from scraped $LaCoO_3$(111) at temperatures of (a) 200 K, (b) 300 K and (c) 450 K. The binding energy scale is as given in (a). Spectra are normalized to the incident photon flux. Dashed lines are drawn from the lowest binding energy resonance minimum in all cases. Delayed resonance onset over the lower part of the binding energy range is seen in (a) and (b), but is absent in (c).

are significantly lower than those of low temperature $LaCoO_3$, lying at similar energies to those for $LaCoO_3$ at around 300–400 K. This appears consistent with table 1 [17], which shows a maximum in the proportion of the IS state in this temperature range, with only a low contribution (8–10%) from the LS state.

3.5. Detailed CIS investigation of feature B as a function of binding energy

In order to separate the contributions of the different spin states to feature B, station 4.1 at the SRS was used in combination with a Scienta 200 mm analyser to investigate CIS profiles taken at small binding energy increments around feature B, as a function of temperature. Figure 11 shows these data, at temperatures of 200 K, 300 K and 450 K, in the binding energy range 0.2–2.2 eV (centred on feature B at around 1.2 eV). The spectra taken at 450 K are relatively straightforward; for binding energies in the range 1.2–2.2 eV, all resonances have the same onset energy of ∼61.8 eV, and there is no significant resonance for binding energies less than 1.2 eV. However, at both 200 K and 300 K, the resonance onset energy changes with binding energy, from ∼62 eV at 2.2 eV binding energy to around 64 eV at 0.7 eV binding energy. Below 0.7 eV, there is no significant resonance. We attribute the changes as a function of temperature to the decreasing contribution of the LS state to feature B as the temperature is raised. The binding energy variation suggests that the maxima in the contributions of the LS and HS/IS states to B occur at slightly different binding energies, as implied by the cluster

calculations (figure 1) [18]. The data taken at 450 K show no delayed onset, and we conclude that the sample is therefore predominantly in higher spin states (HS, IS or mixed HS/IS), i.e. the LS contribution is too small to be detected (as implied by table 1 [17]). The intensities of the CIS spectra suggest that the maximum contribution to feature B from these states is centred at binding energies of around 1.7–2.2 eV. The presence of a delayed resonance onset at 200 K, and residual traces of it at 300 K, indicate the presence of a significant proportion of LS states, centred in the binding energy range 0.7–1.2 eV, i.e. at lower binding energy than the contribution from higher spin states. In the range 1.2–1.7 eV binding energy, we observe a transition from 'normal' to delayed onset. We note that these binding energies are in the reverse order to that expected from calculations (figure 1 [18]), where the HS/IS states give a contribution to B at lower binding energy than the LS states. To some extent this is expected, as the calculation is aligned arbitrarily by its authors, placing the maximum in the LS states at 1 eV [18]. One result is that it incorrectly shows a Fermi level crossing for the IS state, which is known not to occur in practice (i.e. the compound is non-metallic to $\sim$500 K, whereas the calculation as presented indicates it should be metallic). These difficulties have been acknowledged previously. Our results suggest a binding energy minimum for the LS state at low temperature around 1 eV lower that any higher states (HS/IS). We note that this agrees well with the difference in ground state energies calculated by Takahashi and Igarashi [27], although this comparison should be treated with caution, as our spectra are of course representative of the joint DOS of initial and final states, rather than the ground state alone. This experiment provides the basis for the 1 eV shift between LS and HS/IS states introduced in the simulation of the valence band spectra discussed in section 3.3. We note that this yields excellent agreement between experimental and simulated spectra, so the EDC and CIS data appear consistent with each other.

4. Conclusions

Clear temperature effects are seen in the valence band photoemission spectra of single crystal $LaCoO_3$, which may be attributed to changes in the spin state of the sample. These effects are not observed in equivalent spectra from $La_{0.9}Sr_{0.1}CoO_3$, and may also be distinguished from effects due to surface degradation in UHV. The most obvious change is a gradual transition from the LS to other spin states as the temperature is raised. This is clearly identified by a delayed resonance onset in the CIS spectra, which may be used as a 'diagnostic' of the LS state. Our data clearly show that the lowest binding energy feature in the spectra (feature B) is associated with the LS state, but that it also contains contributions from higher spin states. Detailed investigation of this feature using CIS allows us to conclude that the binding energy difference between the LS and HS/IS states in the spectral function at 200 K is around 1 eV. The LS contribution is the lowest binding energy feature.

While the LS state is clearly identified by its delayed resonance, neither HS nor IS states should show a delayed onset. It is therefore difficult to distinguish these two spin states on the basis of their CIS spectra. However, certain features of the EDC spectra are consistent with the existence of an IS state, and with a further gradual transition from it into a HS state as the temperature is raised. In particular, the relative changes in intensity in features B, C and D as a function of temperature appear consistent with a three spin-state model involving the IS state [17]. Simulation of the observed temperature variation, using the proportions of HS, IS and LS states suggested by magnetic susceptibility measurements [17], show excellent agreement with experiment. We therefore conclude that the three state model provides a good description of the valence band data for $LaCoO_3$. In contrast the 10% Sr doped compound is found to be in the same spin state at all temperatures, thought to be an IS spin state [12, 28], as

indicated by the lack of resonance shifts and the unchanging valence band spectra observed as a function of temperature. This confirms that the temperature-dependent effects observed at B in the $LaCoO_3$ spectra are due to depopulation of the LS state, and not attributable to artefacts such as effects of phonon broadening.

Adsorption measurements show that water is chemisorbed on the $LaCoO_3(111)$ surface at low temperatures (possibly with some dissociation). As the sample temperature is raised, the water dissociates completely when the temperature reaches 200 K. The resulting OH does not desorb completely at room temperature. The spectrum is strikingly similar to that from a poorly cleaved surface which has spent some time in UHV, and we therefore conclude that the surface degradation observed on poorly prepared surfaces is associated with hydroxylation of the surface by water in the residual vacuum.

Acknowledgments

We would like to thank John Campbell of CLRC Daresbury Laboratory for the Laué simulations. We thank EPSRC(UK) and National Power plc, Johnson Matthey plc, CLRC Daresbury Laboratory and ICI Katalco for studentships to SW, PMD, DEJ, PGDM and SCG. This work was supported by grant GR/K63030 from the EPSRC, and partly by scientific research grant 08640449 from the Ministry of Education, Sports and Culture, Japan. We also thank S Murata at the University of Electro-Communications for growing the crystals.

References

[1] Hrovat M, Katsarakis N, Reichmann K, Bernik S, Kuscer D and Holc J 1996 *Solid State Ion.* **83** 99
[2] Hollingworth J *et al* 1999 *J. Electron Spectrosc. Relat. Phenom.* **101–3** 765
[3] Yamaguchi S, Taniguchi H, Takagi H, Arima T and Tokura Y 1995 *J. Phys. Soc. Japan* **64** 1885
[4] Briceno G, Xiang X-D, Chang H, Sun X and Schultz P G 1995 *Science* **270** 273
[5] Golovanov V, Mihaly L and Moodenbaugh A R 1996 *Phys. Rev.* B **53** 8207
[6] Raccah P M and Goodenough J B 1967 *Phys. Rev.* **155** 932
[7] Menyuk N, Dwight K and Raccah P M 1967 *J. Phys. Chem. Solids* **28** 549
[8] Heikes R R, Miller R C and Mazelsky R 1964 *Physica* **30** 1600
[9] Blasse G 1965 *J. Appl. Phys.* **36** 879
[10] Jonker G H 1966 *J. Appl. Phys.* **37** 1424
[11] Asai K, Gehring P, Chou H and Shirane G 1989 *Phys. Rev.* B **40** 10 982
[12] Caciuffo R, Rinaldi D, Barucca G, Mira J, Rivas J, Senaris-Rodriguez M A, Radaelli P G, Fiorani D and Goodenough J B 1999 *Phys. Rev.* B **59** 1068
[13] Mira J, Rivas J, Vazquez M, Garcia-Beneytez J M, Arcas J, Sanchez R D and Senaris-Rodriguez M A 1999 *Phys. Rev.* B **59** 123
[14] Yamaguchi S, Okimoto Y, Ishibashi K and Tokura Y 1998 *Phys. Rev.* B **58** 6862
[15] Nam D N H, Jonason K, Nordblad P, Khiem N V and Phuc N X 1999 *Phys. Rev.* B **59** 4189
[16] Itoh M, Sagahara M, Natori I and Motoya K 1995 *J. Phys. Soc. Japan* **64** 3967
[17] Asai K, Yoneda A, Yokokura O, Tranquada J M, Shirane G and Kohn K 1998 *J. Phys. Soc. Japan* **67** 290
[18] Saitoh T, Mizokawa T, Fujimori A, Abbate M, Takeda Y and Takano M 1997 *Phys. Rev.* B **55** 4257
[19] Abbate M, Fuggle J C, Fujimori A, Tjeng L H, Chen C T, Potze R, Sawatzky G A, Eisaki H and Uchida S 1993 *Phys. Rev.* B **47** 16 124
[20] Thornton G, Tolfield B C and Hewat A W 1986 *J. Solid State Chem.* **61** 301
[21] Thornton G, Morrison F C, Partington S, Tolfield B C and Williams D E 1988 *J. Phys. C: Solid State Phys.* **21** 2781
[22] Thornton G, Owen I W and Diakun G P 1991 *J. Phys.: Condens. Matter* **3** 417
[23] Asai K, Yokokura O, Nishimori N, Chou H, Tranquada J M, Shirane G, Higuchi S, Okajima Y and Kohn K 1994 *Phys. Rev.* B **50** 3025
[24] Goodenough J B 1971 *Mater. Res. Bull.* **6** 967
[25] Korotin M A, Yu S, Ezhov, Solovyev I V, Anisimov V I, Khomski D I and Sawatzky G A 1996 *Phys. Rev.* B **54** 5309

[26] Potze R, Sawatzky G A and Abbate M 1995 *Phys. Rev.* B **51** 11 501
[27] Takahashi M and Igarashi J-I 1997 *Phys. Rev.* B **55** 13 557
[28] Saitoh T, Mizokawa T, Fujimori A, Abbate M, Takeda Y and Takano M 1997 *Phys. Rev.* B **56** 1290
[29] Louca D, Sarrao J L, Thompson J D, Röder H and Kwei G H 1999 *Phys. Rev.* B **60** 10 378
[30] Taguchi Y, Ichikawa K, Katsumi T, Jouda K, Ohta Y, Soda K, Kawamata S, Okuda K and Aita O 1997 *J. Phys.: Condens. Matter* **9** 6761
[31] Part of the Lauegen suite, CLRC Daresbury Laboratory. See e.g. Campbell J W 1995 *J. Appl. Crystallogr.* **28** 228
[32] Chainani A, Mathew M and Sarma D D 1992 *Phys. Rev.* B **46** 9976
[33] Zhuang M, Zhang W, Hu C and Ming N 1998 *Phys. Rev.* B **57** 10 710
[34] Flavell W R, Laverty J H, Law D S-L, Linsay R, Muryn C A, Flipse C F J, Raiker G N, Wincott P L and Thornton G 1990 *Phys. Rev.* B **41** 11 623
[35] Masuda S, Aoki M, Harada Y, Hirohashi H, Watanabe Y, Sakisaka Y and Koto H 1993 *Phys. Rev. Lett.* **25** 4214
[36] Vasquez R P 1996 *Phys. Rev.* B **54** 14 938
[37] Munakata F, Takahashi H, Akimune Y, Shichi Y, Tanimura M, Inoue Y, Itti R and Koyama Y 1997 *Phys. Rev.* B **56** 979
[38] Shen Z-X *et al* 1990 *Phys. Rev.* B **42** 1817
[39] Abbate M, Potze R, Sawatzky G A and Fujimori A 1994 *Phys. Rev.* B **49** 7210
[40] Eriksen S, Naylor P D and Egdell R G 1987 *Spectrochim. Acta* A **43** 1535
[41] Siegbahn K 1974 *J. Electron. Spectrosc. Relat. Phenom.* **5** 1
[42] Potter F H and Egdell R G 1993 *Surf. Sci.* **297** 286
[43] Kurtz R L, Stockbauer R, Madey T E, Mueller D, Shih A and Toth L 1988 *Phys. Rev.* B **37** 7936
[44] Lindan P J D, Harrison N M and Gillan M J 1998 *Phys. Rev. Lett.* **80** 762
[45] Brookes N B, Thornton G and Quinn F M 1987 *Solid State Commun.* **64** 383
[46] Cardona M and Ley L 1978 *Photoemission in Solids I, General Principles* ed M Cardona and L Ley (Berlin: Springer)
[47] Yeh J J and Lindau I 1985 *At. Data Nucl. Data Tables* **32** 1